nature portfolio

Peer Review File

Realizing High Power Factor and Thermoelectric Performance in Band Engineered AgSbTe2

Corresponding Author: Dr Yu Zhang

This file contains all reviewer reports in order by version, followed by all author rebuttals in order by version.

Version 0:

Reviewer comments:

Reviewer #1

(Remarks to the Author)
In this study, Zhang et al. present an approach using Sn as an effective dopant to enhance the thermoelectric properties of p-type AgSbTe2. They demonstrate that Sn doping stabilizes AgSbTe2 by inhibiting the formation of n-type Ag2Te. The authors observe an increase in carrier concentration and the emergence of a new impurity band above the valence band maximum, resulting in an improved power factor. Consequently, they report a peak zT value of 2.5 at 673 K and an average zT of 1.32 from 300 K to 673 K. Notably, the team successfully fabricated a thermoelectric unicouple using the optimized AgSbTe2 and Yb0.25Co3.75Fe0.25Sb12, achieving a conversion efficiency of up to 12.1% and a power density of 1.13 W/cm². Given the significant enhancements in material properties and device performance, this work is potentially to attract substantial interest from readers. However, several issues need clarification before publication:

1) Stabilization mechanism: The incorporation of trace amounts of Sn into the cationic sublattice effectively stabilizes the AgSbTe2 matrix. Could the authors elaborate on the underlying mechanisms responsible for this stabilization? Additionally, are there other elements that could potentially have a similar effect?
2) Carrier concentration: The low-temperature carrier concentration results in Fig. S2 appear inconsistent with the high-temperature data in Fig. 4b. Furthermore, the observed decrease in carrier concentration with increasing temperature requires explanation.
3) Carrier concentration and mobility: The variation in carrier concentration and mobility with different levels of Sn doping lacks a clear pattern. The authors are requested to provide a more detailed explanation for this observation.
4) Bipolar diffusion and Seebeck coefficient: Although the Sn-doped samples exhibit bipolar thermal conductivity at high temperatures, indicating the presence of bipolar diffusion, the Seebeck coefficient does not decrease correspondingly. The authors should clarify this phenomenon.
5) zT comparison and data update: A comparison plot of zT values for the current AgSbTe2 material is recommended. Additionally, the main text does not mention Fig. S7, and some data in Fig. S7 do not represent the highest reported values for that material. The authors should update these data to avoid misleading readers.
6) Details on the Thermoelectric unicouple: The manuscript should include detailed information on the preparation and testing of the thermoelectric unicouple to ensure reproducibility. The authors should also provide measurement results of interfacial resistances. Since a unicouple is not a typically practical device, its efficiencies can be challenging to measure accurately. It is strongly recommended that the authors use commercial equipment, such as mini-PEM, to verify the unicouple efficiency and at the same time validate the results through simulation calculations (e.g. Ansys or Comsol).

Minor issues
1) To my knowledge, the mechanical properties of AgSbTe2 are generally poor. Does Sn doping enhance the mechanical properties of AgSbTe2?
2) Please provide the reference for the heat flow equation. Additionally, how did the authors determine the uncertainties in output power and conversion efficiency?

Reviewer #2

(Remarks to the Author)
In this manuscript, the thermoelectric properties of Sn-doped AgSbTe2 were investigated theoretically and experimentally. The study achieved the high power factor and ZT values with the acceptable reproducibility. While the results are

interesting, the supporting data and analysis are insufficient to understand of the Sn-doping effect on the AgSbTe2. In my opinion, the major revision is required to address the following issues.

1. Because the AgSbTe2 has two-types of the carriers, the electron and hole carrier concentrations should be presented using a two-carrier model calculation. This approach would provide more a clear understanding of the Sn-doping effects.

2. The transport properties of the Sn-doped AgSbTe2 of this work differ from those in previous research on the Sn-doped AgSbTe2 [APL Mater. 2, 096114 (2014)]. What accounts for these different behaviors?

3. The TEM results indicate increased disordering of the Sn-doped AgSbTe2. But the lattice thermal conductivities are also enhanced by the Sn-doping. What is the explanation for this phenomenon?

4. The bipolar effect is suppressed by the Sn-doping. What causes this suppression?

5. The AgSbTe2 intrinsically decomposes into the Ag2Te and Sb2Te3 below 633 K. The Sn-doped AgSbTe2 of the thermoelectric module might also decompose into the Ag2Te and Sb2Te3 due to the temperature difference. How long can the thermoelectric module operate stably with the temperature difference of ΔT = 370 K, which shows the conversion efficiency of 12.1%.

Reviewer #3

(Remarks to the Author)
In this manuscript, the authors report that Sn doping can introduce a new impurity band in AgSbTe2, inhibit the bipolar effect, and prevent the formation of Ag2Te. Based on the effects mentioned above, the thermoelectric performance of Sn-doped $AgSbTe_2$ is significantly enhanced, with the ZT value reaching 2.5 at 673 K, which is relatively high. Additionally, the authors fabricated a unicouple TE device, achieving an energy conversion efficiency of 12.1%. Overall, this manuscript is well organized and the data are sufficient to support the final conclusions. This work is worthy of publication as it offers new perspectives for further enhancing the thermoelectric performance of $AgSbTe_2$. I recommend this interesting work for publication after a minor revision.
1. An important effect of Sn doping is the suppression of the bipolar effect in $AgSbTe_2$, which leads to a significant increase in the power factor at high temperatures. However, the authors have not provided a detailed explanation for how Sn doping suppresses the bipolar effect. As mentioned in the manuscript, minority carriers (electrons) thermally excited across the band gap counteract the positive Seebeck coefficients. In other words, the bipolar effect is closely related to the band gap of the material. However, as observed from the band structure in Figure 2, aside from the impurity band introduced by Sn doping, there is little change in the band structure before and after doping. The authors need to provide a more detailed and thorough explanation of the specific mechanism behind this effect.
2. In the Supplementary Materials, the authors provide the testing method for low-temperature Hall resistivity, using a PPMS from 5 K to 300 K up to 9 T. However, on line 265 in manuscript, they report the carrier concentration of $AgSb_{0.94}Sn_{0.06}Te_2$ at 2 K. Which one is correct? Additionally, in Figures 4(b) and (c), why is the carrier concentration and mobility for pristine $AgSbTe_2$ only provided in the 300–400 K range? Why not present the data across the entire temperature range, consistent with the Sn-doped samples?
3. Ag and Sb ions randomly occupy positions within the cation sublattice of $AgSbTe_2$. Sn doping can enhance Ag/Sb ordering and generate the disrupted lattice structure.
Atomic disorder typically plays a crucial role in inducing additional scattering of charge carriers, thereby reducing their mobility. Once the degree of order is enhanced, the mobility should increase. However, undoped AgSbTe2 shows a hole mobility of 288 cm2/Vs, whereas in Sn-doped samples, mobilities plummet to levels as low as 31 cm2/Vs. The authors' explanation for the changes in mobility is not entirely convincing. It is recommended that they conduct a more in-depth discussion and analysis based on the carrier scattering mechanisms.
4. In the manuscript, the authors state that "Cation doping has been frequently used to enhance Ag/Sb ordering, resulting in the appearance of cation-ordered nanoscale domains (2-4 nm) within polycrystalline $AgSbTe_2$ matrices. These nanodomains play a critical role in reducing lattice thermal conductivity." Indeed, the authors also observed a more disrupted structure in Sn-doped $AgSbTe_2$ compared to undoped $AgSbTe_2$. From this perspective, the lattice thermal conductivity of the Sn-doped $AgSbTe_2$ samples should be lower than that of undoped $AgSbTe_2$. However, the opposite trend is shown in Figure 4(h). The authors should provide a detailed discussion and explanation of this in the manuscript.

Version 1:

Reviewer comments:

Reviewer #1

(Remarks to the Author)
The authors have made commendable efforts to improve the work and have added substantial experiments to address my question. However, I still have one minor question:

Regarding device simulation: It is unusual that the simulated power output exceeds the measured power, while the simulated efficiency aligns with the measured efficiency. Could the authors provide a more detailed comparison between

simulated and experimental values, including open-circuit voltage, internal resistance, power, heat flow, and efficiency across different temperature differences? This would offer readers a clearer understanding of the device's performance.

Additionally, please highlight the revisions made in the manuscript, as it is currently difficult for me to identify the updated sections.

Reviewer #2

(Remarks to the Author)
I think that the manuscript is significantly revised and most of critical issues are cleared accordingly.
So, I recommend the publication as in this form.

Reviewer #3

(Remarks to the Author)
The revised manuscript has significantly improved in quality. All concerns have been addressed, and no further revisions are necessary. I therefore recommend this work for publication.

Version 2:

Reviewer comments:

Reviewer #1

(Remarks to the Author)
The author has responded well to my questions and has revised them,So, I recommend the publication as in this form.

Response–to–Referees letter

Reviewer #1:

In this study, Zhang et al. present an approach using Sn as an effective dopant to enhance the thermoelectric properties of p-type $AgSbTe_2$. They demonstrate that Sn doping stabilizes $AgSbTe_2$ by inhibiting the formation of n-type Ag_2Te. The authors observe an increase in carrier concentration and the emergence of a new impurity band above the valence band maximum, resulting in an improved power factor. Consequently, they report a peak zT value of 2.5 at 673 K and an average zT of 1.32 from 300 K to 673 K. Notably, the team successfully fabricated a thermoelectric unicouple using the optimized $AgSbTe_2$ and $Yb_{0.25}Co_{3.75}Fe_{0.25}Sb_{12}$, achieving a conversion efficiency of up to 12.1% and a power density of 1.13 W/cm^2. Given the significant enhancements in material properties and device performance, this work is potentially to attract substantial interest from readers. However, several issues need clarification before publication.

We thank Reviewer #1 for carefully reading through the manuscript and providing insightful comments and important suggestions that helped us improve it. We believe that with the improved manuscript and supporting information, this paper is now clear and convincing. Please find below the detailed response to the received comments.

1. Stabilization mechanism: The incorporation of trace amounts of Sn into the cationic sublattice effectively stabilizes the $AgSbTe_2$ matrix. Could the authors elaborate on the underlying mechanisms responsible for this stabilization? Additionally, are there other elements that could potentially have a similar effect?

The enhanced stability of the $AgSbTe_2$ matrix upon Sn doping can be attributed to two benefits: 1) Reduced Electron Density of Antibonding States: The inherent instability of pristine $AgSbTe_2$ is largely due to the presence of antibonding states near the Fermi level, as proved by crystal orbital Hamiltonian population analysis. The instability arises from the strong hybridization between Sb-5s and Te-5p states, which causes the Te-5p antibonding states to migrate toward the valence band frontier. From an electronic structure perspective, these antibonding contributions constitute the primary states at the top of the valence band, leading to intrinsic instability through the formation of charge-compensated defect complexes. As a result, $AgSbTe_2$ undergoes spontaneous phase decomposition, forming Ag_2Te and Sb_2Te_3 phases for instance. To suppress this instability, Sn doping is an effective strategy to reduce the electron density associated with these antibonding states, thereby enhancing the stability of the $AgSbTe_2$ matrix. Sn^{2+}, with one fewer valence electron than Sb^{3+}, acts as a p-type dopant by introducing additional holes, which efficiently decrease the concentration of electrons associated with the antibonding states, thereby stabilizing the $AgSbTe_2$ structure. The XRD and DSC analysis confirmed that Sn-doped $AgSbTe_2$ exhibits a pure phase with no detectable Ag_2Te impurities.

2) Defect Engineering: In pristine $AgSbTe_2$, defects such as silver vacancies (V_{Ag}) act as acceptors, providing holes to the system. However, the number of V_{Ag} is greatly limited by self-compensating

mechanisms, where donor defects (Sb_{Ag}, Sb atoms occupying Ag sites) form spontaneously to maintain charge neutrality ($V_{Ag}^{1-} + Sb_{Ag}^{1+}$). This self-compensation results in limited hole concentrations and, consequently, unstable $AgSbTe_2$. Sn doping effectively reduces the formation energy of V_{Ag} by promoting the formation of complex defects like ($V_{Ag}^{1-} + Sn_{Sb}^{1-}$), which have a significantly lower formation energy compared to other defects. The preferential formation of these complex defects, regulated by the Sn concentration, leads to a higher hole concentration and enhances the stability of $AgSbTe_2$.

While Sn has proven effective in stabilizing the $AgSbTe_2$ matrix, other elements with similar electronic configurations and defect engineering capabilities could potentially yield comparable results. Elements such as Zn^{2+}, Cd^{2+}, Hg^{2+}, Mg^{2+}, Ca^{2+}, Mn^{2+}, Cu^{2+} and Pb^{2+} can also substitute Sb^{3+} and serve as p-type dopants that modify defect chemistry, thereby stabilizing $AgSbTe_2$ by adjusting the carrier concentration and suppressing the formation of impurity phases. Some of these dopants have already demonstrated effectiveness in phase stabilization and enhancing $AgSbTe_2$ thermoelectric performance (see references listed below). However, the specific impact of each dopant would depend on the precise electronic structure modifications and defect interactions within the doped $AgSbTe_2$ matrix, necessitating further detailed investigations.

Action: The manuscript has been revised accordingly:

"The inherent instability of pristine $AgSbTe_2$ is primarily attributed to the presence of antibonding states near the Fermi level, as proved by crystal orbital Hamiltonian population analysis.[26] The antibonding states arise from the strong hybridization between Sb-5s and Te-5p orbitals, leading to the Te-5p antibonding states shift towards the valence band frontier. From an electronic structure perspective, such antibonding contributions constitute the primary states at the top of the valence band, thereby stimulating intrinsic instability through the formation of charge-compensated defect complexes. Consequently, $AgSbTe_2$ undergoes spontaneous phase decomposition, forming Ag_2Te and Sb_2Te_3 phases for instance. To suppress this instability, p-type doping emerges as an effective strategy to reduce the electron density associated with these antibonding states, thereby potentially enhancing the stability of the $AgSbTe_2$ matrix. To this end, our study aims at stabilizing the $AgSbTe_2$ matrix by incorporating trace amounts of Sn into the cationic sublattice (Figure 1a). The preference for Sn^{2+} to substitute Sb^{3+} is based on its possession of one fewer valence electron, which facilitates the generation of additional holes, thereby contributing to the stabilization of the $AgSbTe_2$ structure." *(Page 5, Line 30)*

"This preferential formation of the complex defects, controlled by the amount of Sn introduced, not only introduces a higher concentration of holes but also enhances the stability of $AgSbTe_2$." *(Page 8, Line 13)*

Reference

1. *ACS Energy Lett. 2017, 2, 349-356* (Zn^{2+})
2. *Science 2021, 371, 722-727* (Cd^{2+})
3. *J. Am. Chem. Soc. 2023, 145, 25392-25400* (Hg^{2+})

4. *ACS Appl. Mater. Interfaces 2023, 15, 9508-9516* (Mg^{2+})
5. *Scientific Reports 2017, 7: 4496* (Ce^{2+})

2. Carrier concentration: The low-temperature carrier concentration results in Fig. S2 appear inconsistent with the high-temperature data in Fig. 4b. Furthermore, the observed decrease in carrier concentration with increasing temperature requires explanation.

We agree with the reviewer that there is a discrepancy in the absolute carrier concentration values presented in Fig. S2 and in Fig. 4b. This difference arises primarily due to the use of two distinct Hall measurements and data process techniques.

For the low-temperature range (2.2-250 K), carrier concentration was determined using the standard four-probe technique in a Physical Properties Measurement System (***PPMS, Quantum Design***) with a magnetic field strength of up to 9 T. This high magnetic field provides a more precise measurement of the Hall voltage, allowing for an accurate determination of carrier concentration, particularly in the presence of complex band structures and multiple carrier types. In contrast, the high-temperature measurements (300-670 K) were conducted using the van der Pauw method in a LakeShore Hall Effect System (***8400 Series HMS, LakeShore***) with a fixed magnetic field of 0.9 T. The van der Pauw method requires thin, homogeneous samples and generally assumes a single dominant carrier type. However, it employs a lower magnetic field, which may introduce variability in the measured Hall coefficient, especially in cases where multiple scattering mechanisms or mixed carrier types are temperature-dependent. Additionally, differences in data processing between the four-probe and van der Pauw methods contribute to discrepancies in carrier concentration values between low- and high-temperature measurements. Detailed explanations of these measurement techniques and carrier concentration calculations are provided in the revised SI section.

Despite the methodological differences and temperature-dependent variations, both measurement techniques consistently reveal a significant increase in hole carrier concentration upon Sn doping. This consistency underscores the role of Sn as an effective p-type dopant in enhancing the carrier concentration in $AgSbTe_2$.

Regarding the observed decrease in carrier concentration with increasing temperature, this phenomenon is associated with the changes in the electronic band structure of Sn-doped $AgSbTe_2$. Temperature elevation modifies the density of states near the band edges thus inducing a shift in the Fermi level. Variations in Sn concentration also leads to the formation of different impurity states or modifications in the valence band, impacting the overall carrier dynamics. Besides, elevated temperatures cause thermal excitation of electrons into the conduction band and carrier trapping by localized states, leading to a reduction in the net carrier concentration.

Action: We have added the following discussions in the revised manuscript:

"*The preferential formation of the complex defects, controlled by the amount of Sn introduced, not only introduces a higher concentration of holes but also enhances the stability of $AgSbTe_2$. This is supported by experimental data on charge carrier density across both low (5-200 K,*

four-probe method, Figure S2 and S3) and high-temperature ranges (300-670 K, van der Pauw method, Figure 4b). While both measurements show the introduction of Sn to increase the hole concentration, the carrier concentrations calculated in the low-temperature range are higher than those in the high-temperature range. This variation is attributed to differences in magnetic field strength and data processing methods between the two measurement techniques." *(Page 8, Line 13)*

"*In addition, elevated temperatures can cause thermal excitation of electrons into the conduction band and carrier trapping by localized states, leading to a reduction in the net carrier concentration in Sn-doped $AgSbTe_2$ with increasing temperature*." *(Page 13, Line 9)*

3. Carrier concentration and mobility: The variation in carrier concentration and mobility with different levels of Sn doping lacks a clear pattern. The authors are requested to provide a more detailed explanation for this observation.

We thank the Reviewer for bringing this point to our attention. As shown in Figure 4b, while all Sn-doped samples exhibit a significant increase in carrier concentration compared to undoped $AgSbTe_2$, the specific doping levels of 3% and 10% Sn show higher carrier concentrations than the 6% Sn-doped sample, reflecting a complex interplay of defect chemistry that is not strictly linear.

Sn doping in $AgSbTe_2$ primarily introduces holes by substituting Sn^{2+} for Sb^{3+} in the cation sublattice. This substitution leads to a deficiency of electrons, effectively increasing the hole carrier concentration. However, the introduction of Sn also affects the formation energy of various defects, including V_{Ag}^{1-}, Sb_{Ag}^{2+}, Sn_{Sb}^{1-}, and compensating defect complexes, such as ($2V_{Ag}^{1-}+Sb_{Ag}^{2+}$), ($Sb_{Ag}^{2+}+Sn_{Sb}^{1-}$), ($2V_{Ag}^{1-}+Sb_{Ag}^{2+}+Sn_{Sb}^{1-}$). These defects and their interactions are sensitive to the Sn doping level, leading to non-monotonic behavior in carrier concentration. At a 3% Sn doping level, the substitution efficiently introduces hole carriers and predominantly forms simple Sn-related defects, resulting in a substantial increase in carrier concentration. However, as the doping concentration increases to 6%, the system may favor the formation of multiple defects and compensating defect complexes, which can partially neutralize the effect of the dopant, thereby reducing the net carrier concentration, or enhanced interactions between impurities might occur, leading to increased carrier scattering and consequently a reduction in carrier concentration. At the higher doping level of 10%, further increases in Sn concentration may introduce local structural distortions in the $AgSbTe_2$ matrix, resulting in changes in the band structure that cause the carrier concentration to increase again. The carrier mobility presents a reverse trend, indicating that mobility is strongly influenced by carrier-carrier scattering and impurity interactions present in the material. The non-monotonic variation in carrier concentration and mobility with different Sn doping levels is a consequence of defect chemistry, defect complex formation, carrier scattering mechanisms, and potential changes in the electronic band structure. These factors collectively govern the nonlinear behavior of carriers in Sn-doped $AgSbTe_2$.

Action: A detailed discussion has been included in the updated manuscript accordingly:

"While Sn doping introduces holes in $AgSbTe_2$, leading to an increase in carrier concentration, as shown in Figure 4b, the effect is non-linear across different doping levels. At a 3% Sn doping level, the substitution efficiently introduces hole carriers and predominantly forms simple Sn-related defects, resulting in a substantial increase in carrier concentration. However, at 6% Sn doping, the emergence of compensating defect complexes, such as like ($2V_{Ag}^{1-} + Sb_{Ag}^{2+}$), ($Sb_{Ag}^{2+} + Sn_{Sb}^{1-}$), ($2V_{Ag}^{1-} + Sb_{Ag}^{2+} + Sn_{Sb}^{1-}$), and enhanced impurity interactions lead to increased carrier scattering and a decrease in net carrier concentration. A high doping level of 10% Sn could introduce significant local structural distortions in the $AgSbTe_2$ matrix, potentially altering the band structure, e.g., shifts in the positions of the conduction band minimum or valence band maximum or even induce changes in the density of states near the Fermi level, that could impact both carrier concentration and mobility. Correspondingly, the carrier mobility presents a reverse trend, indicating that mobility is strongly influenced by carrier-carrier scattering and impurity interactions present in the material."(Page 12, line 9)

4. Bipolar diffusion and Seebeck coefficient: Although the Sn-doped samples exhibit bipolar thermal conductivity at high temperatures, indicating the presence of bipolar diffusion, the Seebeck coefficient does not decrease correspondingly. The authors should clarify this phenomenon.

We appreciate the Reviewer's observation regarding the bipolar behavior of the Seebeck coefficient in Sn-doped $AgSbTe_2$ samples. Typically, the presence of bipolar diffusion, which contributes to bipolar thermal conductivity (κ_{bi}), negatively impacts the Seebeck coefficient due to the opposing contributions from thermally excited minority carriers.

In this work, the contribution of κ_{bi} in undoped $AgSbTe_2$ becomes apparent after heating to 450 K as illustrated in the Figure S5 (presented below), and quickly increasing to 0.25 W/mK at 660 K. Upon Sn doping, a significant reduction in the bipolar conductivity was observed. The κ_{bi} decrease from 0.25 W/mK in pristine $AgSbTe_2$ to 0.07 W/mK in Sn-doped $AgSbTe_2$ at 660 K, demonstrating more than 70% decreasing. This phenomenon can be attributed to one main factor: the substitution of Sb^{3+} with Sn^{2+} significantly increases the hole concentration, thereby enhancing the overall p-type behavior of the material. Sn^{2+}, with one fewer valence electron compared to Sb^{3+}, introduces extra holes. Additionally, Sn doping increases the concentration of Ag vacancies, which further contribute to hole generation. Moreover, Sn doping reduces the occurrence of Sb_{Ag}^{2+} antisite defects, which would otherwise generate electrons, thereby weakening their negative contribution to the Seebeck coefficient.

In addition, from the Hall data obtained using PPMS (Figure S3), it can be observed that with increasing magnetic field strength, the value of Hall resistivity (ρ_{xy}) in pristine $AgSbTe_2$ first decreases slowly to a minimum and then gradually increases (Figure S3a). This effect becomes more pronounced as the temperature rises, particularly above 50 K. The sign of the slope ($k = \rho_{xy}/\mu_o H$) serves as an indicator of the dominant charge carrier: a negative slope ($k<0$) suggests electron dominance, while a positive slope ($k>0$) points to hole dominance. As the magnetic field

strength increases, the slope of each curve transfers from negative to positive, as marked by the red arrow in Figure S3. Notably, at 300 K, the slope remains negative even under high magnetic fields (3-5 T), confirming that electrons dominate transport in pristine $AgSbTe_2$ at this temperature. Upon Sn doping, a significant change in the shape of the curves is clearly observed in Figure S3b and S3c compared to the undoped $AgSbTe_2$. For the doped samples, the ρ_{xy} value monotonically increases with the magnetic field strength, with the slope k consistently remaining positive. This evidently indicates that Sn doping shifts the dominant charge carrier from electrons to holes, supporting the above hypothesis that Sn^{2+} acts as an effective p-type dopant in $AgSbTe_2$. Afterwards, the concentrations of both electrons and holes were estimated using a two-carrier model and present in Figure S3, which demonstrate a significant suppress in electron concentration (minor carrier) upon Sn doping. This result further supports our conclusion that Sn doping not only enhances hole concentration but also suppresses the bipolar effect by increasing the n_h/n_e ratio.

Besides, the maintained Seebeck coefficient can also be attributed to changes in the electronic band structure induced by Sn doping. Specifically, Sn doping results in band flattening and significant band splitting at the Γ point (Figure 2b), which increases the effective mass (m^*) of the charge carriers. An increased m^* is beneficial for maintaining relatively high Seebeck coefficients, even in the presence of minor bipolar diffusion.

As a result, due to the substantial reduction in n_e and enhanced m^*, the Seebeck coefficient does not exhibit a decrease in the temperature range measured. Nevertheless, we do observe a detention in its upward trend within the temperature range of 450-600 K, which can be attributed to the interplay between the increased m^* and the dominance of majority carriers (holes), which counteract the influence of minority carriers.

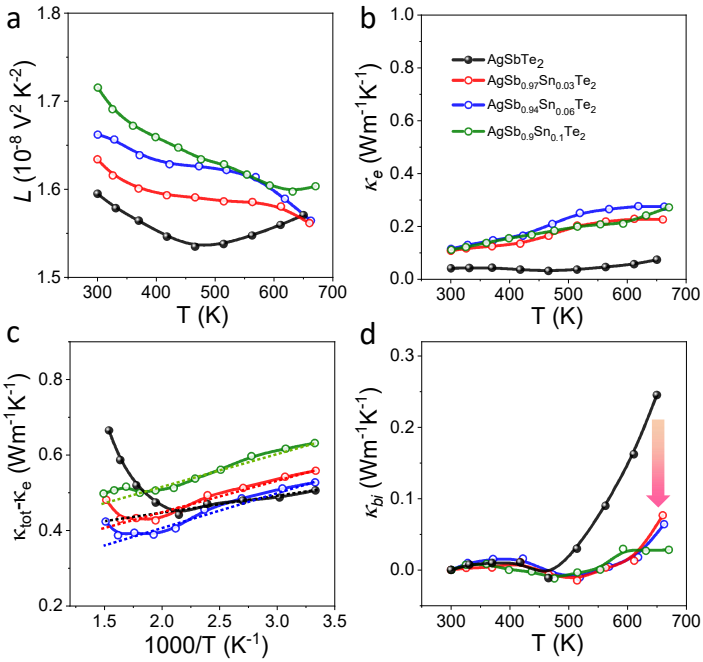

Figure S5. Temperature dependence of (a) Lorenz number, L; (b) electronic thermal conductivity (κ_e); (c) Subtraction of the electronic thermal conductivity from total thermal conductivity (κ_{tot}-κ_e) and (d) bipolar thermal conductivity (κ_{bi}) of polycrystalline $AgSb_{1-x}Sn_xTe_2$ samples.

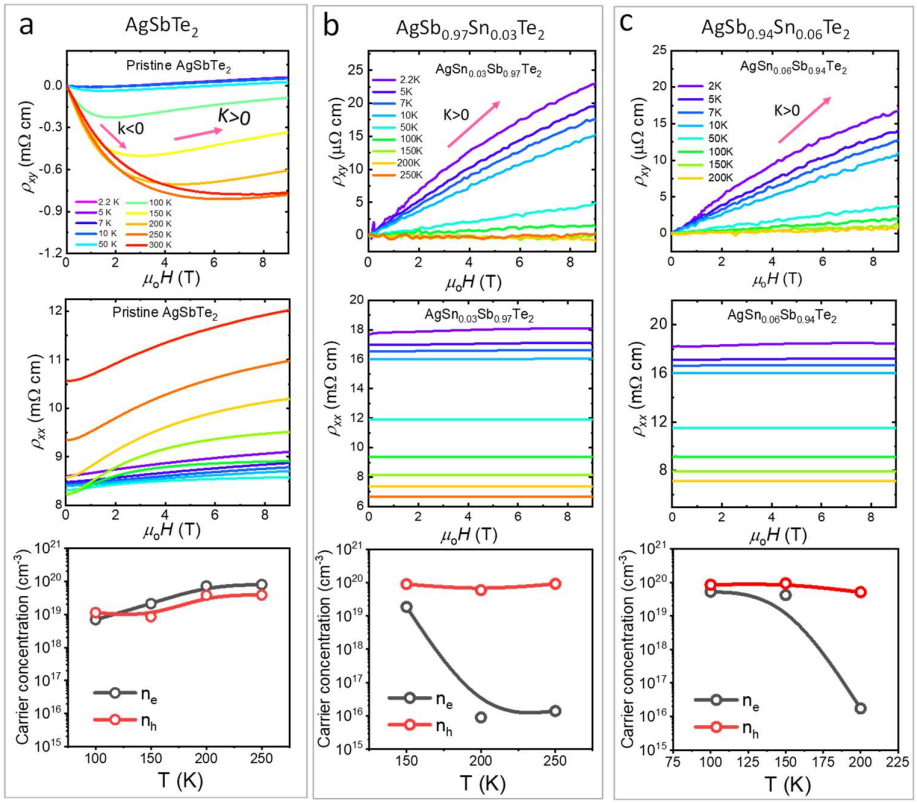

Figure S3. Representative field-dependent Hall resistivity (ρ_{xy}), longitudinal resistivity (ρ_{xx}) and calculated concentration of electrons (n_e) and holes (n_h) by two band model at different temperatures. (A) pristine $AgSbTe_2$; (B) $AgSb_{0.97}Sn_{0.03}Te_2$ sample; (C) $AgSb_{0.94}Sn_{0.06}Te_2$ sample.

Action: The figures and corresponding discussions have been included in the updated manuscript accordingly:

"The introduction of Sn resulted in a reduction in the Seebeck coefficient due to the increased charge carrier concentration. However, the doped samples still demonstrated decent Seebeck coefficients values, exceeding 170 μV/K across the entire temperature range, as shown in Figure 4d. Although the upward trend of the Seebeck coefficient in the Sn-doped samples was moderated, a mild increase was still observed beyond 460 K, attributed to a significant reduction in the bipolar effect. While bipolar conduction was not entirely suppressed, it was substantially reduced compared to pristine $AgSbTe_2$. The sustained Seebeck coefficients stem primarily from the significant decrease in electrons and the alteration in band structure upon

Sn doping, characterized by band flattening and splitting, thereby inducing an increased m conducive to sustaining relatively high Seebeck coefficients."* (*Page 13, Line 13*)

"In pristine $AgSbTe_2$, the hole concentration (n_h) presents consistently lower values than the electron concentration (n_e) when T>100 K (Figure S3), aligning with previous reports of negative Hall coefficients in $AgSbTe_2$ at room temperature.[16] However, upon Sn doping, a significant increase in hole concentration was observed, reaching 9×10^{19} cm^{-3} in $AgSb_{0.97}Sn_{0.03}Te_2$ sample, with all doped samples showing higher n_h than n_e." (*Page S9, Line 14*)

5. *zT* comparison and data update: A comparison plot of *zT* values for the current AgSbTe2 material is recommended. Additionally, the main text does not mention Fig. S7, and some data in Fig. S7 do not represent the highest reported values for that material. The authors should update these data to avoid misleading readers.

Following the Reviewer's suggestion, we have updated the summary of zT values for state-of-the-art thermoelectric materials as a function of temperature, ensuring that the data presented are the most accurate and up-to-date (Figure S6). Additionally, we have included a comparison of the zT values for the current $AgSbTe_2$ materials in Figure S7. Both figures have been referenced in the revised manuscript to enhance clarity and avoid potential misinterpretation.

Action: A detailed discussion has been included in the updated manuscript accordingly:

"*The enhanced carrier concentration and sustained high Seebeck coefficients in $AgSb_{0.94}Sn_{0.06}Te_2$ yielded exceptional zT values, reaching a peak of 2.5 and an average zT of 1.32 over the 300-673 K range (Figure 4i). A zT of ~2.5 is among one of the highest values compared with the existing state-of-the-art thermoelectric materials (Figure S6, S7), highlighting the potential of $AgSbTe_2$ for high-efficiency thermoelectric applications in mid-temperature range.*" (*Page 14, Line 29*)

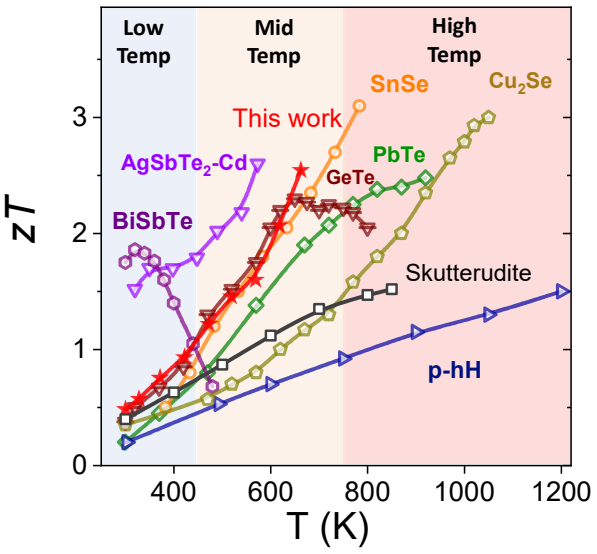

Figure S6. *zT* comparison with state-of-art TE materials across low-, middle- and high-temperature regimes.[11,17-23]

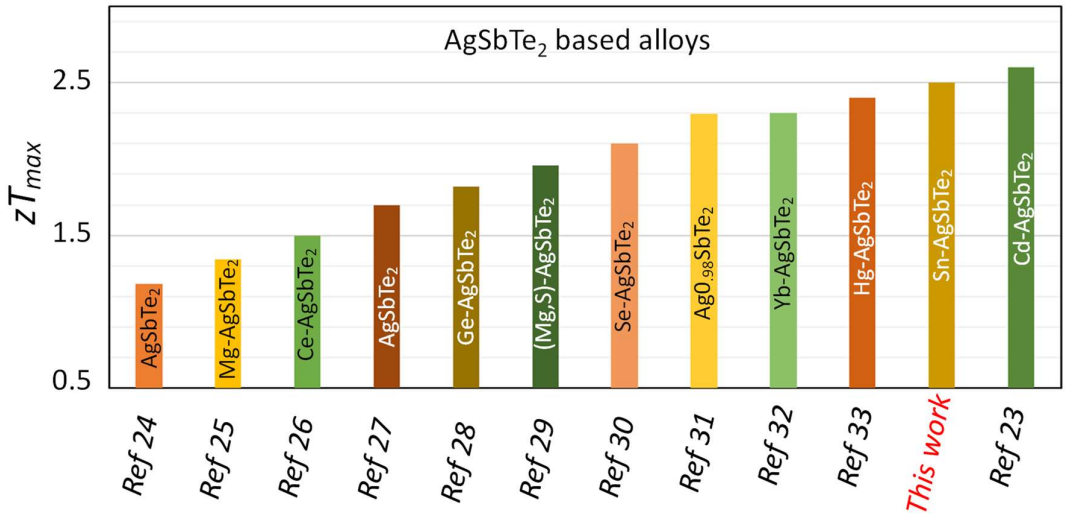

Figure S7. Comparison of the maximum figure of merit, zT_{max}, of $AgSb_{0.94}Sn_{0.06}Te_2$ with other reported $AgSbTe_2$-based materials.[23-33]

6. Details on the Thermoelectric unicouple: The manuscript should include detailed information on the preparation and testing of the thermoelectric unicouple to ensure reproducibility. The authors should also provide measurement results of interfacial resistances. Since a unicouple is not a typically practical device, its efficiencies can be challenging to measure accurately. It is strongly recommended that the authors use commercial equipment, such as mini-PEM, to verify the unicouple efficiency and at the same time validate the results through simulation calculations (e.g. Ansys or Comsol).

As suggested by the Reviewer, we have included additional details on the preparation and testing of the thermoelectric unicouple in the experimental section of the updated Supplementary Information as below:

"*The p-type $AgSb_{0.94}Sn_{0.06}Te_2$ leg, with Ni as diffusion-barrier layers and Cu as electrodes, was fabricated by firstly spark plasma sintering the powders of $AgSb_{0.94}Sn_{0.06}Te_2$ at 703 K under a pressure of 40 MPa for 2 minutes. The obtained bulk pellet was polished and cleaned thoroughly by ultrasonic stirring. The pellet was then diced along the press direction into a certain dimension (P-leg: 2.7 mm (length) × 2.9 mm (width) × 4.8 mm (height)) legs using a wire saw. The reported $Yb_{0.25}Co_{3.75}Fe_{0.25}Sb_{12}$ skutterudite material by Li et al.[10] was used as the n-type leg. The pellet was then diced along the press direction into a certain dimension leg (N-leg: 1.9 mm (length) × 1.4 mm (width) × 4.8 mm (height)) using a wire saw. The obtained bulk pellet was polished and cleaned in ethanol thoroughly by ultrasonic stirring. Afterward, a layer of Ni was deposited on the top and bottom side of each leg by electroless nickel plating*

(~20 µm). The legs were connected by direct bond copper substrates using Gallium-Indium eutectic metal to provide electrical and thermal contact at the junction of thermoelectric leg/header. The output properties of the fabricated unicouple device were measured using a custom-built power generation setup. The measurement method and the testing principle have been explained in our previous works.[8,9,11-13] *The schematic diagram of measurement is described in Figure S9. The output power and conversion efficiency of the unicouple TEGs were simultaneously measured under vacuum condition (~10^{-9} Torr) from room temperature to 400ºC. The hot side temperature was precisely controlled by a heater that provides constant heat flow (Q_{in}) to the top side of the module. TEG converts a portion of this heat into output power (P_{out}) and rejects the rest (Q_{out}) into the Q-meter which is connected to a water-cooled heat sink (cold side) with constant temperature of ~20ºC. The open circuit voltage (V_{oc}) and device voltage (V_d) were recorded at a certain current using a voltmeter (KEITHLEY) and a power supply (KEITHLEY 2200-20-5). Using this information, internal resistance (R_i) and P_{out} were then calculated. The temperatures of hot and cold side were monitored using K-type thermocouples. The system was calibrated thoroughly to minimize the heat loss.* " (Page 19, line 24)

Interface Resistance: As suggested by the Reviewer, we measured the contact resistance using an automated scanning four-probe technique (see insert in Figure S14). The results show a linear increase in resistance with distance, with no evidence of diffusion or significant contact resistance at the interfaces. This confirms an ultra-low ohmic contact resistance between the Cu electrode and the $AgSb_{0.94}Sn_{0.06}Te_2$ leg, with a specific contact resistance for the p-type TE leg of less than $<1\mu\Omega.cm^2$. Such low contact resistance effectively minimizes Joule heating at the TE leg/Cu electrode interface, thereby enhancing thermal-to-electrical energy conversion efficiency. Additionally, the output voltage (V_{oc}) as a function of ΔT, depicted in Figure S13, increases linearly with ΔT, further validating the low contact resistance of the fabricated device.

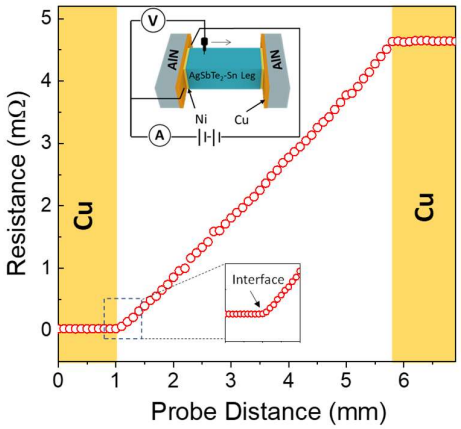

Figure S14. The schematic diagram of home-made four-probe contact resistance measurement system and the contact resistance plots of $AgSb_{0.94}Sn_{0.06}Te_2$ leg.

Commercial Measurement: While we currently do not have access to a Mini-PEM system, our custom-built setup has been employed successfully in numerous studies on unicouple TEGs [*Nature commun., 2023, 14, 3300; Adv. Mater., 2023, 35(20): 2210407; Mater. Today, 2020, 36, 63-72.; Adv. Mater., 2023, 35, 2208994; Adv. Energy Mater., 2020, 10, 2001924*]. To ensure the reliability of our setup, we also performed measurements on a Bi_2Te_3-based unicouple, using commercial n-type and p-type bismuth telluride legs (1.5 × 1.5 × 1.5 mm, *crystalltherm.com*). The results obtained were compared with reported data and demonstrated a strong agreement, confirming the accuracy and reliability of our custom-built setup.

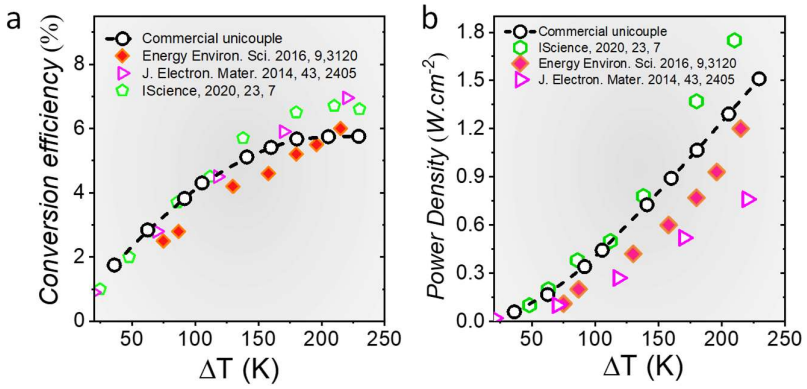

Figure S14-2. (a) Conversion efficiency and (b) output power density of the fabricated Bi_2Te_3 unicouple module compared with state-of-the-art modules.

COMSOL Simulation: Following the Reviewer's recommendation, we conducted simulations of the unicouple module performance using COMSOL Multiphysics 6.2. The simulation was based on a p-type $AgSb_{0.94}Sn_{0.06}Te_2$ leg paired with an n-type skutterudite $Yb_{0.25}Co_{3.75}Fe_{0.25}Sb_{12}$ leg. We incorporated the thermoelectric effects, electrical and thermal contact resistances, and temperature-dependent material properties to ensure accurate modeling. The details of the simulation are provided in the updated Supplementary Information. In the simulation, the cold side temperature was fixed at 300 K, while the hot side temperature was varied to maintain a similar temperature gradient. The simulation results (Figure S16) show slightly higher but comparable values for P_{max}, η_{max} and power density compared with the experimental data, confirming the reliability of the measurements in our study.

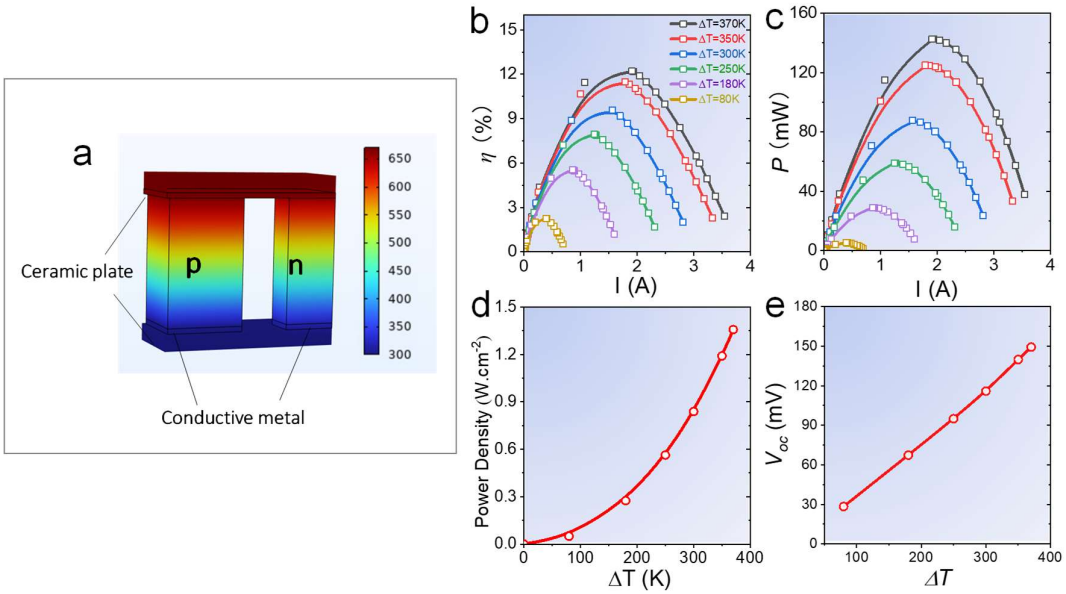

Figure S16. (a) Schematic illustration of the simulated unicouple device made of $AgSb_{0.94}Sn_{0.06}Te_2$ leg and $Yb_{0.25}Co_{3.75}Fe_{0.25}Sb_{12}$ leg. (b) Simulated current-dependent conversion efficiency (η_{max}) and (c) output power (P_{max}) of the unicouple. (d) Simulated maximum power density and (e) open circuit voltage as a function of ΔT.

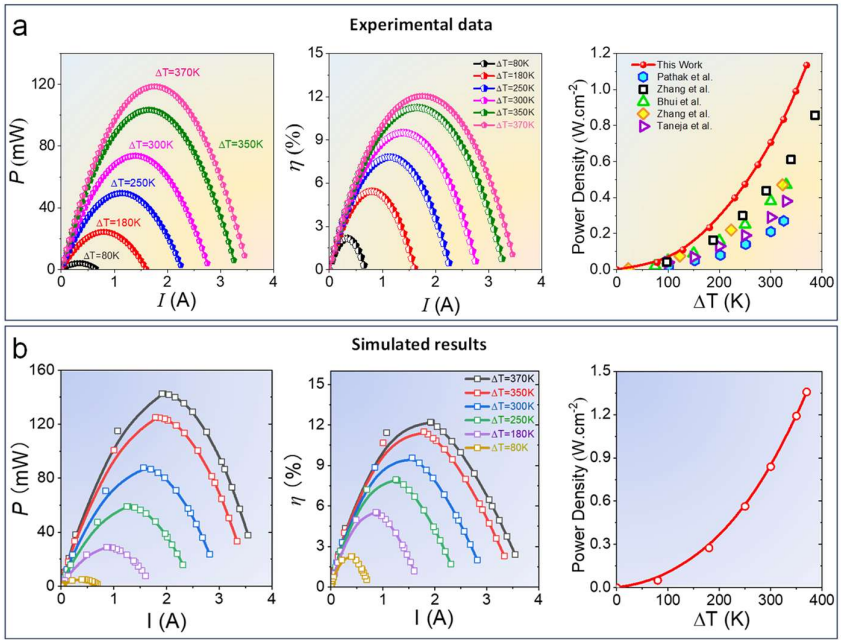

Figure S16-2. Comparison of (A) experimental data with (B) the data from COMSOL Multiphysics simulation software on the unicouple device made of $AgSb_{0.94}Sn_{0.06}Te_2$ leg and $Yb_{0.25}Co_{3.75}Fe_{0.25}Sb_{12}$ leg.

Action: The manuscript and SI have been revised accordingly.

"With a fixed cold-side temperature at 300 K, the open-circuit voltage (V_{oc}) exhibited a linear increase with ΔT (Figure S13), indicating low contact resistance in the fabricated device, as confirmed by automated scanning four-probe measurements (Figure S14). The results demonstrate an ultra-low ohmic contact resistance (<1 μΩ·cm^2) between the Cu electrode and the thermoelectric legs."(*Page 15, Line 13*)

"Device performance was further validated by simulations of current-dependent P_{out} and η, based on the p/n leg dimensions and transport properties. The simulations (Figure S16) showed slightly higher but comparable values for P_{max}, η_{max}, and power density compared to experimental data, confirming the reliability of the measurements." (*Page 16, Line 4*)

Minor issues

1. To my knowledge, the mechanical properties of $AgSbTe_2$ are generally poor. Does Sn doping enhance the mechanical properties of AgSbTe2?

To address the Reviewer's concern, we conducted nanoindentation tests to analyze the mechanical properties, specifically the hardness, of pristine and Sn-doped $AgSbTe_2$. The Vickers hardness values are shown in Figure S17. Both samples displayed similar hardness. Notably, $AgSbTe_2$ exhibits higher hardness than conventional Bi_2Te_3-based alloys, but is significantly softer than $CoSb_3$ and half-Heusler alloys.

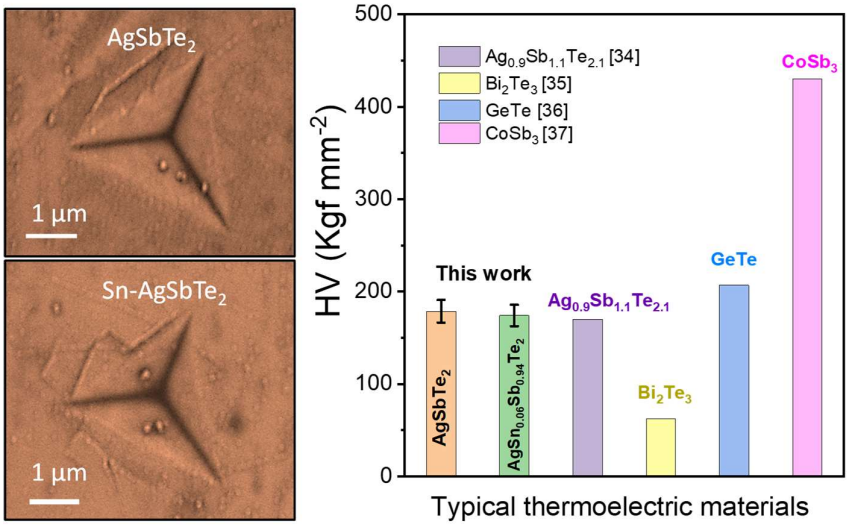

Figure S17. Comparisons on the Vickers hardness for $AgSbTe_2$ and $AgSb_{0.94}Sn_{0.06}Te_2$ with several typical TE materials. The Vickers hardness data are taken from references.[34-37]

2. Please provide the reference for the heat flow equation. Additionally, how did the authors determine the uncertainties in output power and conversion efficiency?

The reference of the heat flow equation is provided according to the reviewer's suggestion. Uncertainties in output power and conversion efficiency: the TE module is measured three times and the average values are reported. The maximum standard deviation of conversion efficiency based on three measurement results is used as uncertainties of conversion efficiency and output power.

Action: The manuscript has been revised accordingly.

"*The maximum power output from TE modules P_{max} (P_{out}) is calculated using the expression:*

$$P_{max} = \frac{V_{oc}^2}{4R_i}$$

where V_{oc} is the measured open-circuit voltage and R_i is the module internal resistance. V_{oc} and device voltage (V_d) were recorded at a certain current using a voltmeter (KEITHLEY) and a power supply (KEITHLEY 2200-20-5). The heat flow (Q_{out}) of unicouple decive is calculated by:

$$Q_{out} = Q_{leg(p)} + Q_{leg(n)} = \kappa_p \times \frac{A_p}{l_p} \times \Delta T + \kappa_n \times \frac{A_n}{l_n} \times \Delta T$$

where κ, A and ΔT are the thermal conductivity, cross-section area, and temperature difference of TE legs, respectively. Q_{rad} is defined as $Q_{rad} = Q'_{out} - Q_{out}$, where Q'_{out} is measured and calculated from a copper Q-meter which is connected to a water-cooled heatsink. Thermal radiation (Q_{rad}) is determined negligible when ΔT<420 K in our previous study,[8,9] therefore, in this study, Q_{out} is used to represent the heat flow through the TE module.

The conversion efficiency of double-leg modules is quantified by:

$$\eta = \frac{P_{out}}{Q_{in}} = \frac{P_{out}}{Q_{out} + P_{out}}$$

where Q_{in} represents the heat flow from heat source. The TE module is measured three times and the average values are reported. The maximum standard deviation of conversion efficiency based on three measurement results is used as uncertainties of conversion efficiency and output power."

Reviewer #2:

In this manuscript, the thermoelectric properties of Sn-doped $AgSbTe_2$ were investigated theoretically and experimentally. The study achieved the high-power factor and ZT values with the acceptable reproducibility. While the results are interesting, the supporting data and analysis are insufficient to understand of the Sn-doping effect on the $AgSbTe_2$. In my opinion, the major revision is required to address the following issues.

We greatly appreciate the Reviewer for the valuable comments and suggestions on our manuscript. We have carefully addressed each of the points raised and made significant revisions to the manuscript and SI based on the Reviewer's feedback. As a result, we have improved the quality of the manuscript and believe that it is now ready for publication.

1. Because the $AgSbTe_2$ has two-types of the carriers, the electron and hole carrier concentrations should be presented using a two-carrier model calculation. This approach would provide more a clear understanding of the Sn-doping effects.

We agree with the Reviewer that the $AgSbTe_2$ contains two-types of carriers. From the data obtained using the Physical Property Measurement System (Figure S3), it can be observed that with increasing magnetic field strength, the value of Hall resistivity (ρ_{xy}) in pristine $AgSbTe_2$ first decreases slowly to a minimum and then gradually increases (Figure S3a). This effect becomes more pronounced as the temperature rises, particularly above 50 K. The sign of the slope ($k = \rho_{xy}/\mu_o H$) serves as an indicator of the dominant charge carrier: a negative slope ($k<0$) suggests electron dominance, while a positive slope ($k>0$) points to hole dominance. As the magnetic field strength increases, the slope of each curve transfers from negative to positive, as marked by the red arrow in Figure S3. Notably, at 300 K, the slope remains negative even under high magnetic fields (3-5 T), confirming that electrons dominate transport in pristine $AgSbTe_2$ at this temperature. Despite undoped $AgSbTe_2$ being a p-type material, the experimentally measured Hall coefficient (R_H) turns out to be negative, similar to previous reports (*Phys. Rev. B Condens. Matter Mater. Phys. 2008, 77, 245204; Chem. Mater., 2010, 22, 5521*). Upon Sn doping, a significant change in the shape of the curves is clearly observed in Figure S3b and S3c compared to the undoped $AgSbTe_2$. For the doped samples, the ρ_{xy} value monotonically increases with the magnetic field strength, with the slope k consistently remaining positive. This evidently indicates that Sn doping shifts the dominant charge carrier from electrons to holes, supporting the hypothesis that Sn^{2+} acts as an effective p-type dopant in $AgSbTe_2$.

Following the Reviewer's suggestion and based on the experimental data presented above, the concentrations of both electrons and holes were estimated using a two-carrier model to evaluate the impact of Sn doping on electronic transport:[14,15]

$$\sigma_{xy} = \frac{\rho_{xy}}{\rho_{xx}^2 + \rho_{xy}^2} = \left[\frac{-n_e \mu_e^2}{1 + (\mu_e B)^2} + \frac{n_h \mu_h^2}{1 + (\mu_h B)^2}\right] eB$$

It is important to note that accurately fitting both ρ_{xy} and ρ_{xx} at each temperature was challenging, as the precision relies on the two-carrier model developed. To address this, we provided 'best-fit' plots for both hole and electron concentrations in Figure S3, which demonstrate a significant increase in hole concentration upon Sn doping. This result further supports our conclusion that Sn doping not only enhances hole concentration but also suppresses the bipolar effect by increasing the n_h/n_e ratio, as outlined in the manuscript. We have incorporated this figure and the corresponding discussion into the revised version, and we thank the reviewer for the constructive feedback, which has helped us clarify the carrier dynamics in Sn-doped $AgSbTe_2$ system.

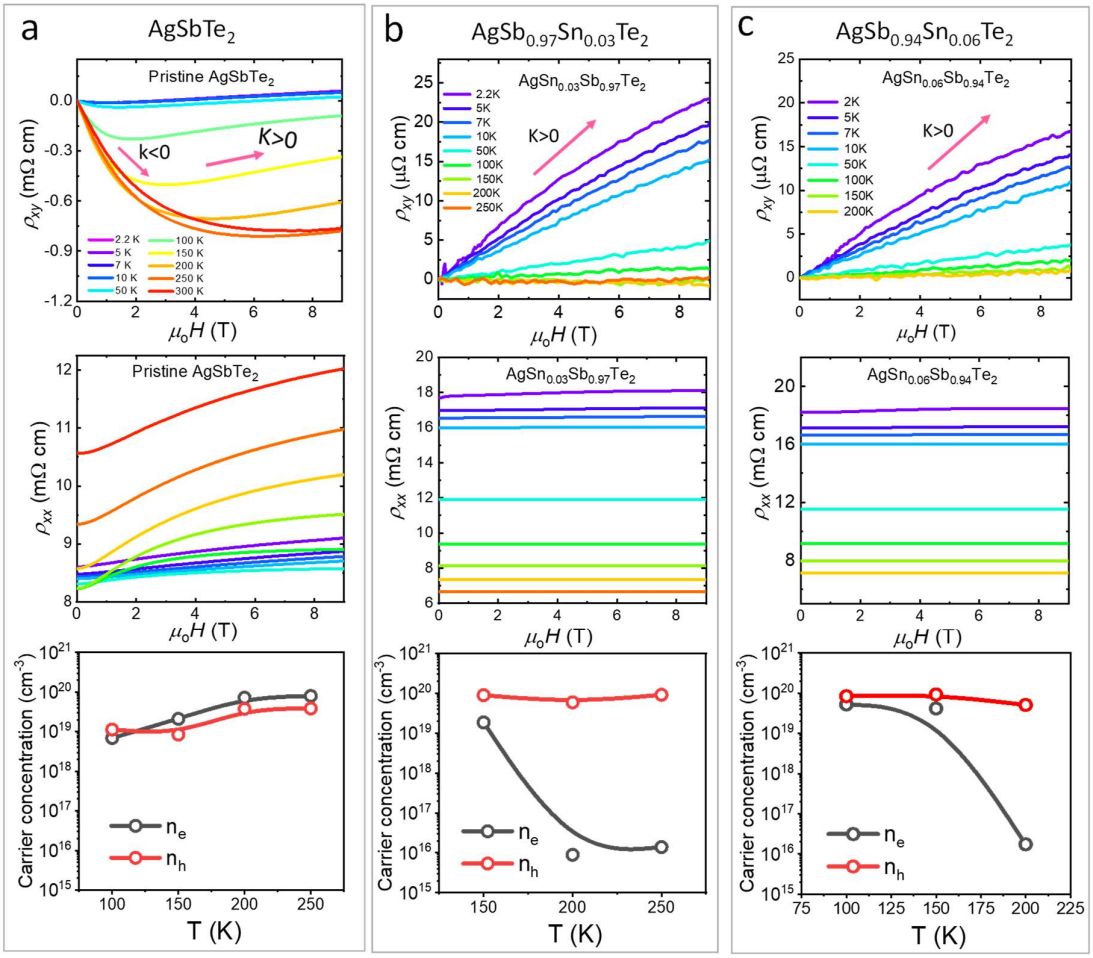

Figure S3. Representative field-dependent Hall resistivity (ρ_{xy}), longitudinal resistivity (ρ_{xx}) and calculated concentration of electrons (n_e) and holes (n_h) by two band model at different temperatures. (A) pristine $AgSbTe_2$; (B) $AgSb_{0.97}Sn_{0.03}Te_2$ sample; (C) $AgSb_{0.94}Sn_{0.06}Te_2$ sample.

"*Given that $AgSbTe_2$ contains two types of carriers, the accurate concentrations of electrons and holes requires two-carrier model to evaluate the impact of Sn doping on each carrier. The concentrations of both electrons and holes were estimated using two-carrier model and equation from previous works*[14,15]*.*

$$\sigma_{xy} = \frac{\rho_{xy}}{\rho_{xx}^2 + \rho_{xy}^2} = \left[\frac{-n_e \mu_e^2}{1 + (\mu_e B)^2} + \frac{n_h \mu_h^2}{1 + (\mu_h B)^2}\right] eB$$

Where ρ_{xx}, ρ_{xy} and B are longitudinal resistivity, Hall resistivity and magnetic field strength measured from PPMS. In pristine $AgSbTe_2$, the hole concentration (n_h) presents consistently lower values than the electron concentration (n_e) when T>100 K (Figure S3), aligning with previous reports of negative Hall coefficients in $AgSbTe_2$ at room temperature.[16] However, upon Sn doping, a significant increase in hole concentration was observed, reaching 9×10^{19} cm^{-3} in $AgSb_{0.97}Sn_{0.03}Te_2$ sample, with all doped samples showing higher n_h than n_e." (*Page S4, Line 7*)

2. The transport properties of the Sn-doped $AgSbTe_2$ of this work differ from those in previous research on the Sn-doped $AgSbTe_2$ [*APL Mater. 2, 096114 (2014)*]. What accounts for these different behaviors?

We thank the Reviewer for bringing this paper to our attention. We have carefully reviewed the referenced work [*Mohanraman et al. APL Mater. 2, 096114 (2014)*] to identify the factors contributing to the discrepancies in transport properties. Our analysis highlights three critical differences:

1) Sn Solubility: In our study, we achieved a significantly higher Sn solubility (~10 at%) compared to the maximum solubility of 3 at% reported by *Mohanraman et al.* This discrepancy likely arises from differences in the synthesis methods employed. *Mohanraman et al.* utilized the Bridgman method, which may lead to an inhomogeneous distribution of dopants within the $AgSbTe_2$ matrix, potentially limiting solubility. In contrast, our synthesis approach-combining a melting method with ball milling and spark plasma sintering (SPS)-ensured a more uniform mixing of Sn atoms within the matrix.

2) Carrier Concentration and Doping Mechanism: *Mohanraman et al.* observed a decrease in carrier concentration with Sn doping, from 1.38×10^{20} cm^{-3} in undoped $AgSbTe_2$ to 0.26×10^{20} cm^{-3} in $AgSb_{0.99}Sn_{0.01}Te_2$. However, in our work, we report an increase in hole carrier density upon Sn doping. As discussed in our manuscript, this increase can be attributed to the substitution of Sb^{3+} ($5s^25p^3$) by Sn^{2+} ($5s^25p^2$), which introduces additional holes into the system. Moreover, Sn doping enhances the formation of Ag vacancies, which further contribute to hole generation. The key difference likely arises from the Hall data processing techniques. *Mohanraman et al.* report a bipolar effect at lower Sn doping levels, suggesting the need for a two-carrier model to accurately assess carrier concentrations. Additionally, the baseline carrier concentration in their undoped sample (1.38×10^{20} cm^{-3}) is notably higher than values typically reported for $AgSbTe_2$ in the literature (*Science 371, 722–727 (2021); J. Am. Chem. Soc., 145, 25392-25400 (2023); Adv. Funct. Mater. 2024, 2400679; ACS Appl. Mater. Interfaces 2023, 15, 9508-9516; Energy Environ. Sci., 2023, 16, 3110*).

This discrepancy emphasizes the complexity of accurately determining carrier concentrations and suggests that subtle variations in synthesis conditions could significantly influence carrier behavior.

3) Ag_2Te Impurity Phase: Due to the inherent instability of $AgSbTe_2$, and the presence of the Ag_2Te impurity phase has been commonly reported in undoped $AgSbTe_2$, irrespective of synthesis methods. The *APL Mater.* work, however, reports a pure $AgSbTe_2$ phase in the undoped sample, which deviates from the findings of numerous other studies. In contrast, the study claims that the Ag_2Te phase appears after doping with 5-7% Sn, whereas our work and other studies consistently observe the Ag_2Te phase in undoped $AgSbTe_2$ samples, which can significantly influence the transport properties.

These discrepancies might stem from differences in sample preparation, synthesis conditions, or processing techniques, all of which are known to affect the microstructure, phase stability, and consequently the transport properties of $AgSbTe_2$-based materials. Despite the observed differences, both works contribute valuable insights into the modification of electrical transport properties in $AgSbTe_2$ by Sn doping.

Action: A related discussion has been included in the revised manuscript:

"*It is worth noting that one previous work[53] also explored Sn doping in $AgSbTe_2$, but key differences in carrier density, bipolar conduction, and impurity phases were observed compared to our work and recent studies,[13, 14, 17, 19, 20] which significantly impact transport properties, leading to distinct thermoelectric performance.*" (*Line 14, Page 24*)

3. The TEM results indicate increased disordering of the Sn-doped $AgSbTe_2$. But the lattice thermal conductivities are also enhanced by the Sn-doping. What is the explanation for this phenomenon?

We appreciate the reviewer's observation regarding the lattice thermal conductivity in Sn-doped $AgSbTe_2$. It is crucial to emphasize that undoped $AgSbTe_2$ already exhibits inherently low, glass-like thermal conductivity, primarily due to its highly chaotic structure. This is associated with the presence of a significant number of stacking faults and dislocations, which effectively scatter medium- and low-frequency acoustic phonons. Additionally, undoped $AgSbTe_2$ contains a large number of nanosized Ag_2Te impurity phases and line defects, as reported in previous works. These cumulative effects result in an ultralow lattice thermal conductivity of ~0.5 W/m·K in undoped $AgSbTe_2$ at room temperature.

Upon Sn doping, the Ag_2Te impurity phase was completely removed from $AgSbTe_2$ matrix, which plays a critical role in the observed increase in lattice thermal conductivity, despite the continued structural disorder. The absence of this impurity phase, which previously enhanced phonon scattering, may reduce the effectiveness of phonon scattering mechanisms in the Sn-doped material, thus leading to higher lattice thermal conductivity. Additionally, it is important to note that the doping element itself can significantly influence phonon transport behavior. While previous studies with Cd/Hg/Yb doping showed a decrease in lattice thermal conductivity, our

findings suggest that Sn doping might introduce different interactions within the matrix that contribute to the observed enhancement in thermal conductivity. This highlights the importance of the specific dopant in determining the material's overall phonon transport characteristics.

Action: The following discussion has been included in the updated manuscript:

"*The total thermal conductivity (κ) of pristine $AgSbTe_2$ initially decreases with increasing temperature, dropping from 0.55 W/m·K at 300 K to 0.48 W/m·K around 450 K (Figure 4g), and then increased. This rise in thermal conductivity is attributed to the contribution of bipolar thermal conductivity (κ_{bi}), as illustrated in Figure 4h and S5. The inherently low thermal conductivity of pure $AgSbTe_2$ aligns with previous studies that identify it as exhibiting glass-like ultralow intrinsic thermal conductivity, attributed to the strong anharmonicity in the defects, stacking faults, and spontaneously formed nanoscale impurity phase.*[6, 7, 15, 18, 20] *In contrast, Sn-doped $AgSbTe_2$ demonstrates higher κ values compared to the pristine material. This increase is primarily due to enhanced electronic thermal conductivity (κ_e) and a slight elevation in κ_L. The increase in κ_L can be attributed to the elimination of the nanostructed Ag_2Te impurity phase upon Sn doping, which reduces phonon scattering centers and consequently allows for more efficient heat transport through the lattice. While previous studies on Hg,*[21] *Yb,*[22] *and Cd*[20] *doping in $AgSbTe_2$ have reported decreases in lattice thermal conductivity, our study observes an increase in κ_L suggesting that the specific nature of the doping element and its interactions within the matrix play a critical role in determining the overall thermal behavior.*" (*Line 13, Page 31*)

4. The bipolar effect is suppressed by the Sn-doping. What causes this suppression?

Generally, the suppression of bipolar conduction can be achieved via two primary strategies: (i) increasing the band gap, as observed with Mg or Mn alloying in PbTe (*Energy Environ. Sci., 2013, 6, 3346; Energy Environ. Sci., 2018, 11, 2486*), or (ii) enhancing the ratio of majority to minority carriers, such as through Pb doping in p-type Bi_2Te_3 to increase hole concentration (*Materials 2017,10,763*; *J. Mater. Res. Technol., 2021, 14, 639*).

In this work, we demonstrate that Sn doping in $AgSbTe_2$ effectively suppresses the bipolar effect by significantly increasing the ratio of majority carriers (n_h) to minority carriers (n_e). This occurs through the substitution of Sb^{3+} with Sn^{2+}, which introduces additional holes since Sn^{2+} has one fewer valence electron compared to Sb^{3+}. Additionally, Sn doping increases the concentration of V_{Ag}^{1-}, which act as acceptors, further contributing to hole generation. This is achieved by lowering the formation energy of V_{Ag}^{1-}, thereby enhancing their presence. Moreover, Sn doping reduces the concentration of Sb_{Ag}^{2+} antisite defects, which would otherwise generate electrons, thereby

suppressing the self-compensating effect. The cumulative effect leads to a significant increase in the net n_h/n_e ratio, which effectively reduces the bipolar conduction.

The calculated n_e and n_h data by two carrier model presented in Figure S3, corroborate the notable suppression of n_e (minority carriers) upon Sn doping. Moreover, we observe a substantial decrease in the bipolar thermal conductivity (κ_{bi}), from 0.25 W/mK in pristine $AgSbTe_2$ to 0.07 W/mK in Sn-doped $AgSbTe_2$ at 660 K (Figure S5). The reduction in κ_{bi} clearly indicates the efficacy of hole doping in suppressing the bipolar conductivity.

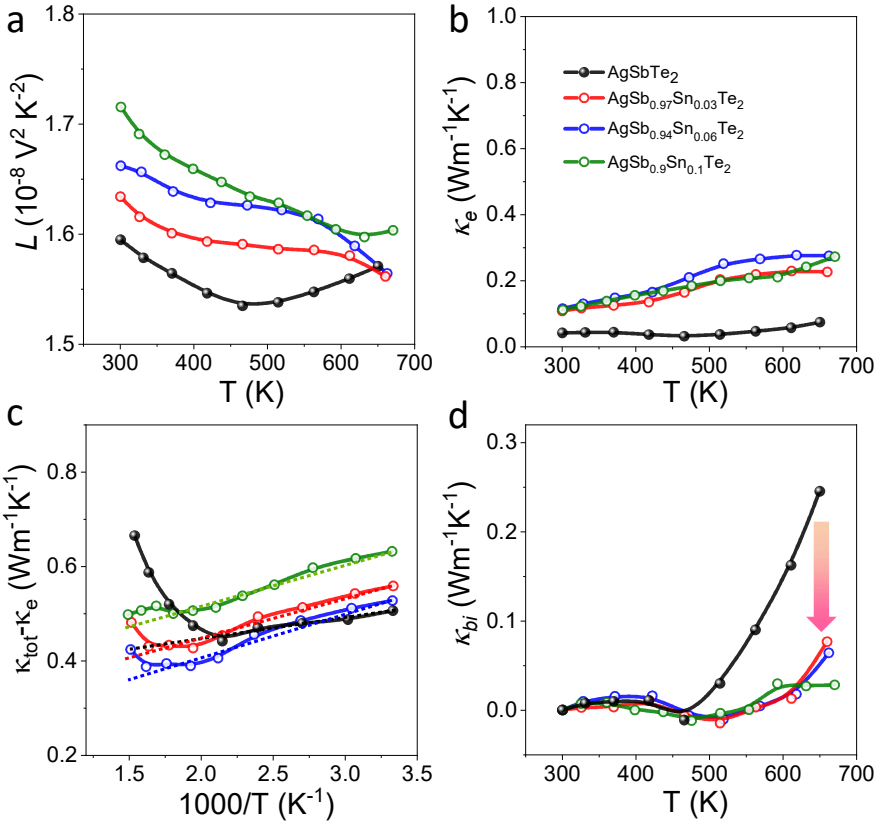

Figure S5. Temperature dependence of (a) Lorenz number, L; (b) electronic thermal conductivity (κ_e); (c) Subtraction of the electronic thermal conductivity from total thermal conductivity (κ_{tot}-κ_e) and (d) bipolar thermal conductivity (κ_{bi}) of polycrystalline $AgSb_{1-x}Sn_xTe_2$ samples.

Action: A detailed explanation has been included into the revised manuscript:

"*Besides, upon partial substitution of Sn for Sb in $AgSbTe_2$, although complete suppression of the bipolar effect was not achieved, a significant reduction in the bipolar thermal conductivity κ_{bi} was observed. Sn doping in $AgSbTe_2$ reduces the bipolar effect by increasing the ratio of majority carriers (holes) to minority carriers (electrons). This occurs through the substitution of Sb^{3+} with Sn^{2+}, which introduces additional holes, increases the concentration of V_{Ag}^{1-} that act as acceptors, and reduces Sb_{Ag}^{2+} antisite defects that would otherwise generate electrons,*

resulting in a higher n_h/n_e ratio and reduced bipolar conduction. The decrease in κ_{bi}, from 0.25 W/mK in pristine $AgSbTe_2$ to 0.07 W/mK in Sn-doped $AgSbTe_2$ at 660 K (Figure S5), underscores the role of increased n_h/n_e in reducing the detrimental bipolar contribution." (Page 14, Line 14)

5. The $AgSbTe_2$ intrinsically decomposes into the Ag_2Te and Sb_2Te_3 below 633 K. The Sn-doped $AgSbTe_2$ of the thermoelectric module might also decompose into the Ag_2Te and Sb_2Te_3 due to the temperature difference. How long can the thermoelectric module operate stably with the temperature difference of ΔT = 370 K, which shows the conversion efficiency of 12.1%.

We appreciate the Reviewer's concern regarding the intrinsic phase instability of $AgSbTe_2$, particularly its tendency to decompose into Ag_2Te and Sb_2Te_3 below 633 K. This decomposition poses a significant challenge for the long-term application of $AgSbTe_2$-based materials.

There are two primary considerations for ensuring the practical use of $AgSbTe_2$-based materials in TE applications: a) supressing the formation of Ag_2Te and Sb_2Te_3 phases during synthesis, and, b) maintaining stability during long term thermal cycling.

1) Suppressing Ag_2Te and Sb_2Te_3 formation through compostional engineering: The first critical step involves the purification of the $AgSbTe_2$ matrix to minimize Ag_2Te impurity formation. Our research, along with other studies, demonstrates that compositional engineering via doping can effectively enhance the structural integrity of $AgSbTe_2$. Specifically, doping with Sn has been demonstrated to significantly reduce the formation of undesirable secondary phases. The Sn dopant modifies the carrier density and reduces the formation of charge-compensating defects, which are known to drive decomposition in pure $AgSbTe_2$. In particular, Sn doping reduces the electron density in antibonding states, thereby suppressing the formation of impurity phases, enhancing the material's overall phase stability post synthesis.

2) Long-term stability: Regarding the stability of Sn-doped $AgSbTe_2$ under thermal conditions, we performed comparative studies on the thermal stability of pristine $AgSbTe_2$ versus Sn-doped $AgSb_{0.94}Sn_{0.06}Te_2$. Spark plasma sintered samples were subjected to annealing in an argon atmosphere for 72 hours at 673 K. XRD analysis post-annealing indicated that the pristine $AgSbTe_2$ exhibited significant phase decomposition, with prominent formation of Ag_2Te and Sb_2Te_3 (Figure S10a). In contrast, the Sn-doped $AgSb_{0.94}Sn_{0.06}Te_2$ sample retained its XRD pattern (Figure S10b), demonstrating remarkable phase stability, even after prolonged thermal exposure. We also tested the cyclic performance of the $AgSb_{0.94}Sn_{0.06}Te_2$-based unicouple module across a ΔT of 370 K over ten thermal cycles. The module exhibited only a minor reduction in efficiency, confirming its robustness under thermal cycling conditions (Figure S10c).

However, we acknowledge the inherent phase instability of $AgSbTe_2$, as indicated by the phase diagram, which suggests decomposition below 633 K after extended exposure. While our findings show improved stability in Sn-doped $AgSbTe_2$, further investigation into long-term operational stability is warranted. Future work could focus on employing additional stabilizing techniques, such as thermal cycling treatments, to improve the material's resistance to phase decomposition.

Notably, previous studies have reported that thermal cycling can induce the precipitation of Ag nanoparticles and redistribute Ag_2Te within the matrix, which in turn stabilizes the material and improves TE performance (*Adv. Funct. Mater. 2024, 2404886; Adv. Mater. 2024, 2409275*). Exploring such mechanisms can offer valuable strategies for extending the lifetime and reliability of $AgSbTe_2$-based thermoelectric modules.

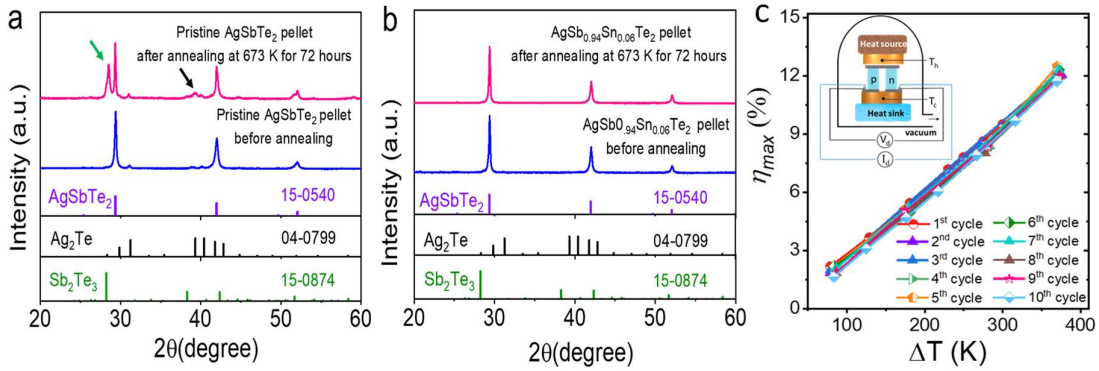

Figure S10. XRD patterns of (a) pristine $AgSbTe_2$ and (b) $AgSb_{0.94}Sn_{0.06}Te_2$ samples before and after annealing in argon atmosphere at 673 K for 72 hours. (c) Cyclic test on the unicouple device after thermal cycling between 373 K and 673 K for ten cycles.

Action: The manuscript and Si has been revised accordingly.

"The inherent instability of pristine $AgSbTe_2$ is primarily attributed to the presence of antibonding states near the Fermi level, as proved by crystal orbital Hamiltonian population analysis.[26] The antibonding states arise from the strong hybridization between Sb-5s and Te-5p orbitals, leading to the Te-5p antibonding states shift towards the valence band frontier. From an electronic structure perspective, such antibonding contributions constitute the primary states at the top of the valence band, thereby stimulating intrinsic instability through the formation of charge-compensated defect complexes. Consequently, $AgSbTe_2$ undergoes spontaneous phase decomposition, forming Ag_2Te and Sb_2Te_3 phases for instance. To suppress this instability, p-type doping emerges as an effective strategy to reduce the electron density associated with these antibonding states, thereby potentially enhancing the stability of the $AgSbTe_2$ matrix. To this end, our study aims at stabilizing the $AgSbTe_2$ matrix by incorporating trace amounts of Sn into the cationic sublattice (Figure 1a). The preference for Sn^{2+} to substitute Sb^{3+} is grounded in its possession of one fewer valence electron, thereby facilitating the generation of additional holes to stabilize the $AgSbTe_2$ structure." (*Page 5, Line 30*)

"In addition, thermal treatment and cyclic performance assessments revealed a significant enhancement in the thermal stability of the Sn-doped materials and devices (Figure S16).

Future studies could focus on evaluating the material's stability over extended periods, which is crucial for the practical application and reliability of TE devices." (*Page 16, Line 7*)

Reviewer #3:

In this manuscript, the authors report that Sn doping can introduce a new impurity band in $AgSbTe_2$, inhibit the bipolar effect, and prevent the formation of Ag_2Te. Based on the effects mentioned above, the thermoelectric performance of Sn-doped $AgSbTe_2$ is significantly enhanced, with the ZT value reaching 2.5 at 673 K, which is relatively high. Additionally, the authors fabricated a unicouple TE device, achieving an energy conversion efficiency of 12.1%. Overall, this manuscript is well organized and the data are sufficient to support the final conclusions. This work is worthy of publication as it offers new perspectives for further enhancing the thermoelectric performance of $AgSbTe_2$. I recommend this interesting work for publication after a minor revision.

We thank Reviewer #3 for his/her appreciations and compliments towards our work, as well as for giving additional suggestions to uplift the comprehensiveness of the manuscript further. With the revisions and additional supporting information, we believe the paper is now clearer and more compelling. Please find our detailed responses to the comments below.

1. An important effect of Sn doping is the suppression of the bipolar effect in $AgSbTe_2$, which leads to a significant increase in the power factor at high temperatures. However, the authors have not provided a detailed explanation for how Sn doping suppresses the bipolar effect. As mentioned in the manuscript, minority carriers (electrons) thermally excited across the band gap counteract the positive Seebeck coefficients. In other words, the bipolar effect is closely related to the band gap of the material. However, as observed from the band structure in Figure 2, aside from the impurity band introduced by Sn doping, there is little change in the band structure before and after doping. The authors need to provide a more detailed and thorough explanation of the specific mechanism behind this effect.

We thank the Reviewer for bringing this point to our attention. Generally, the suppression of bipolar conduction can be achieved via two primary strategies: (i) increasing the band gap, as observed with Mg or Mn alloying in PbTe (*Energy Environ. Sci., 2013, 6, 3346; Energy Environ. Sci., 2018, 11, 2486*), or (ii) enhancing the ratio of majority to minority carriers, such as through atomic doping in p-type Bi_2Te_3 to increase hole concentration (*Materials 2017,10,763*; *J. Mater. Res. Technol., 2021, 14, 639*). In this work, we demonstrate that Sn doping in $AgSbTe_2$ effectively suppresses the bipolar effect by significantly increasing the ratio of majority carriers (n_h) to minority carriers (n_e). This occurs through the substitution of Sb^{3+} with Sn^{2+}, which introduces additional holes since Sn^{2+} has one fewer valence electron compared to Sb^{3+}. Additionally, Sn doping increases the concentration of V_{Ag}^{1-}, which act as acceptors, further contributing to hole generation. This is achieved by lowering the formation energy of V_{Ag}^{1-}, thereby enhancing their presence. Moreover, Sn doping reduces the concentration of Sb_{Ag}^{2+} antisite defects, which would otherwise generate electrons, thereby suppressing the self-compensating effect. The cumulative effect leads to a significant increase in the net n_h/n_e ratio, which effectively reduces the bipolar conduction. The calculated n_e and n_h data by two carrier model presented in Figure S3, corroborate the notable suppression of n_e (minority carriers) upon Sn doping. Moreover, we observe a substantial decrease

in the bipolar thermal conductivity (κ_{bi}), from 0.25 W/mK in pristine $AgSbTe_2$ to 0.07 W/mK in Sn-doped $AgSbTe_2$ at 660 K (Figure S5). The reduction in κ_{bi} clearly indicates the efficacy of hole doping in suppressing the bipolar conductivity.

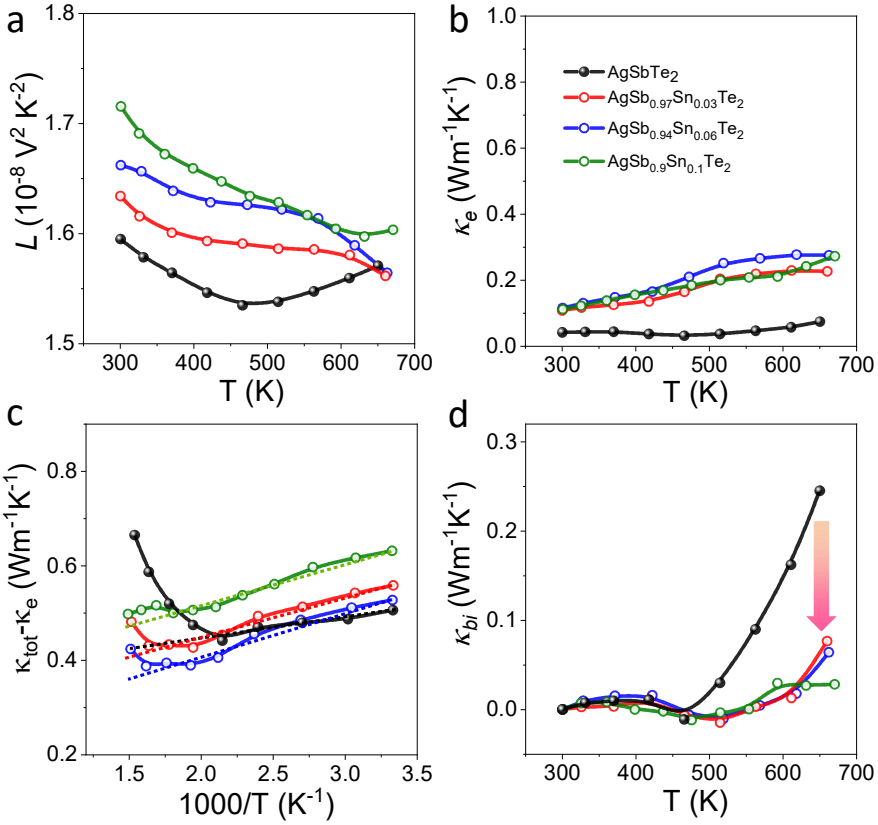

Figure S5. Temperature dependence of (a) Lorenz number, L; (b) electronic thermal conductivity (κ_e); (c) Subtraction of the electronic thermal conductivity from total thermal conductivity (κ_{tot}-κ_e) and (d) bipolar thermal conductivity (κ_{bi}) of polycrystalline $AgSb_{1-x}Sn_xTe_2$ samples.

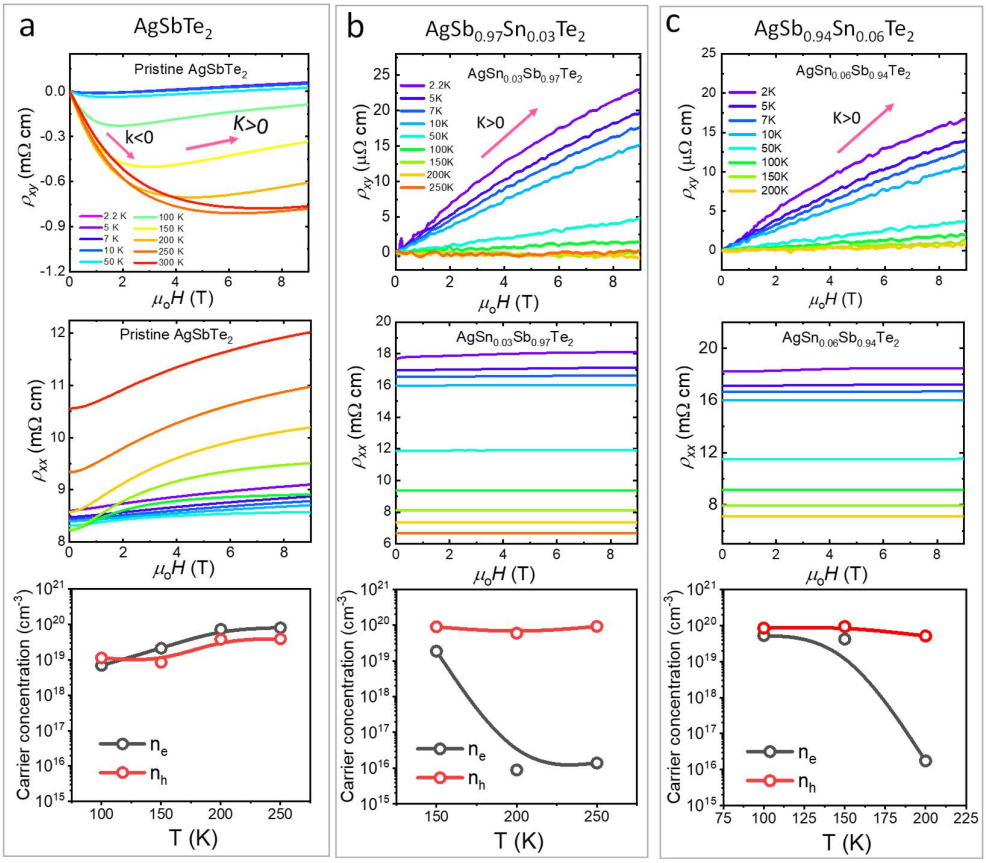

Figure S3. Representative field-dependent Hall resistivity (ρ_{xy}), longitudinal resistivity (ρ_{xx}) and calculated concentration of electrons (n_e) and holes (n_h) by two band model at different temperatures. (A) pristine $AgSbTe_2$; (B) $AgSb_{0.97}Sn_{0.03}Te_2$ sample; (C) $AgSb_{0.94}Sn_{0.06}Te_2$ sample.

Action: The revised manuscript now includes the above figures along with a comprehensive explanation:

"*Besides, upon partial substitution of Sn for Sb in $AgSbTe_2$, although complete suppression of the bipolar effect was not achieved, a significant reduction in the bipolar thermal conductivity κ_{bi} was observed. Sn doping in $AgSbTe_2$ reduces the bipolar effect by increasing the ratio of majority carriers (holes) to minority carriers (electrons). This occurs through the substitution of Sb^{3+} with Sn^{2+}, which introduces additional holes, increases the concentration of V_{Ag}^{1-} that act as acceptors, and reduces Sb_{Ag}^{2+} antisite defects that would otherwise generate electrons, resulting in a higher n_h/n_e ratio and reduced bipolar conduction. The decrease in κ_{bi}, from 0.25 W/mK in pristine $AgSbTe_2$ to 0.07 W/mK in Sn-doped $AgSbTe_2$ at 660 K (Figure S5), underscores the role of increased n_h/n_e in reducing the detrimental bipolar contribution.*" (Page 14, Line 14)

2. In the Supplementary Materials, the authors provide the testing method for low-temperature Hall resistivity, using a PPMS from 5 K to 300 K up to 9 T. However, on line 265 in manuscript, they report the carrier concentration of $AgSb_{0.94}Sn_{0.06}Te_2$ at 2 K. Which one is correct? Additionally, in Figures 4(b) and (c), why is the carrier concentration and mobility for pristine $AgSbTe_2$ only provided in the 300-400 K range? Why not present the data across the entire temperature range, consistent with the Sn-doped samples?

We apologize for the typo error in the manuscript. The low-temperature PPMS measurement was performed from 2.2 K to 250 K, which has been corrected in the updated Supplementary Materials.

Regarding the data for carrier concentration and mobility in pristine $AgSbTe_2$, the reason we only present data in the 300-400 K range in Figure 4 is due to the presence of an impurity phase, Ag_2Te, in the pristine $AgSbTe_2$ samples. Ag_2Te undergoes a structural phase transition around 425 K, which significantly affects carrier transport behavior. Including data beyond 400 K for pristine $AgSbTe_2$ may introduce complexities and uncertainties related to this phase transition. For clarity, we have provided the data for pristine $AgSbTe_2$ from 400 K to 600 K in the updated supplementary information for comparison.

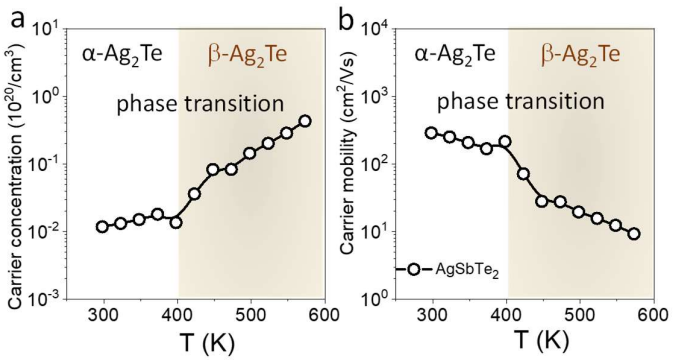

Figure S18. (a) Hall carrier concentration and (b) mobility of at temperatures 300-600 K in undoped $AgSbTe_2$.

3. Ag and Sb ions randomly occupy positions within the cation sublattice of $AgSbTe_2$. Sn doping can enhance Ag/Sb ordering and generate the disrupted lattice structure. Atomic disorder typically plays a crucial role in inducing additional scattering of charge carriers, thereby reducing their mobility. Once the degree of order is enhanced, the mobility should increase. However, undoped $AgSbTe_2$ shows a hole mobility of 288 cm^2/Vs, whereas in Sn-doped samples, mobilities plummet to levels as low as 31 cm^2/Vs. The authors' explanation for the changes in mobility is not entirely convincing. It is recommended that they conduct a more in-depth discussion and analysis based on the carrier scattering mechanisms.

We appreciate the reviewer's insightful comments on the relationship between Ag/Sb ordering and carrier mobility in Sn-doped $AgSbTe_2$. Enhanced ordering within the cation sublattice is indeed expected to reduce atomic disorder, thereby decreasing scattering and potentially increasing mobility. However, the observed reduction in mobility in Sn-doped samples requires consideration of the interplay among carrier concentration and various scattering mechanisms.

In this study, pristine $AgSbTe_2$ exhibits a relatively low carrier concentration of approximately 1.2×10^{18} cm^{-3} and a high hole mobility of ~288 cm^2/Vs at room temperature. Upon Sn doping ($AgSb_{0.94}Sn_{0.06}Te_2$), the carrier concentration dramatically increases nearly 30-fold to $\sim 3.5 \times 10^{19}$ cm^{-3}. However, this increase in carrier concentration is accompanied by a moderate decrease in mobility, with room-temperature hole mobility dropping to ~31 cm^2/Vs.

This reduction in mobility, despite the enhanced Ag/Sb ordering, can be attributed to the complex interplay of multiple scattering mechanisms. While improved cation ordering reduces disorder-related scattering, the significant increase in carrier concentration introduces additional carrier-carrier scattering, which becomes a dominant factor at these elevated concentrations. The mobility degradation observed in Sn-doped samples aligns with trends reported in previous studies on enhanced Ag/Sb atomic ordering (*Science 2021, 371, 722*), where high carrier concentrations lead to increased Coulombic interactions among carriers, thereby reducing mobility. Furthermore, Sn doping generates a large number of complex defects which contribute to enhanced phonon scattering, further limiting carrier mobility. The cumulative effect of these scattering mechanisms-despite the improved cationic ordering-results in the observed decrease in mobility. In conclusion, while Sn doping enhances cation ordering, the simultaneous increase in carrier concentration and the introduction of complex defects create competing scattering mechanisms that more than offset the potential mobility gains from reduced disorder. This intricate balance between different types of scattering is crucial to understanding the mobility behavior in Sn-doped $AgSbTe_2$.

As a result, we have included a detailed discussion in the updated manuscript:

"*Atomic disorder typically plays a crucial role in inducing additional scattering of charge carriers, thereby reducing their mobility.*[42-44] *The enhance Ag/Sb atomic ordering by Sn doping should decrease scattering and potentially increase mobility. In pristine* $AgSbTe_2$*, the carrier concentration is relatively low, around* 1.2×10^{18} cm^{-3}*, while the hole mobility is high, approximately 288* cm^2/Vs *at room temperature. However, upon Sn doping, the carrier concentration increases to* $\sim 3.5 \times 10^{19}$ cm^{-3}*. This substantial increase in carrier concentration is accompanied by a moderate decrease in mobility, with room-temperature carrier mobility dropping to ~31* cm^2/Vs *(Table S1). While Sn doping improves cation ordering, the concurrent rise in carrier concentration and the introduction of complex defects generate competing scattering mechanisms that more than offset the potential mobility gains from reduced disorder*"
(Page 11, Line 9)

4. In the manuscript, the authors state that "Cation doping has been frequently used to enhance Ag/Sb ordering, resulting in the appearance of cation-ordered nanoscale domains (2-4 nm) within polycrystalline $AgSbTe_2$ matrices. These nanodomains play a critical role in reducing lattice thermal conductivity." Indeed, the authors also observed a

more disrupted structure in Sn-doped $AgSbTe_2$ compared to undoped $AgSbTe_2$. From this perspective, the lattice thermal conductivity of the Sn-doped $AgSbTe_2$ samples should be lower than that of undoped $AgSbTe_2$. However, the opposite trend is shown in Figure 4(h). The authors should provide a detailed discussion and explanation of this in the manuscript.

We agree with the reviewer's observation regarding the lattice thermal conductivity in Sn-doped $AgSbTe_2$. It is crucial to emphasize that undoped $AgSbTe_2$ already exhibits inherently low, glass-like thermal conductivity, primarily due to its highly chaotic structure. This is associated with the presence of a significant number of stacking faults and dislocations, which effectively scatter medium- and low-frequency acoustic phonons. Additionally, undoped $AgSbTe_2$ contains a large number of nanosized Ag_2Te impurity phases and line defects, as reported in previous works. These cumulative effects result in an ultralow lattice thermal conductivity of ~0.5 W/m·K in undoped $AgSbTe_2$ at room temperature.

Upon Sn doping, the Ag_2Te impurity phase was completely removed from $AgSbTe_2$ matrix, which plays a critical role in the observed increase in lattice thermal conductivity, despite the continued structural disorder. The absence of this impurity phase, which previously enhanced phonon scattering, may reduce the effectiveness of phonon scattering mechanisms in the Sn-doped material, thus leading to higher lattice thermal conductivity. Additionally, it is important to note that the doping element itself can significantly influence phonon transport behavior. While previous studies with Cd/Hg/Yb doping showed a decrease in lattice thermal conductivity, our findings suggest that Sn doping might introduce different interactions within the matrix that contribute to the observed enhancement in thermal conductivity. This highlights the importance of the specific dopant in determining the material's overall phonon transport characteristics.

Action: The following discussion has been included in the updated manuscript:

"*The total thermal conductivity (κ) of pristine $AgSbTe_2$ initially decreases with increasing temperature, dropping from 0.55 W/m·K at 300 K to 0.48 W/m·K around 450 K (Figure 4g), and then increased. This rise in thermal conductivity is attributed to the contribution of bipolar thermal conductivity (κ_{bi}), as illustrated in Figure 4h and S5. The inherently low thermal conductivity of pure $AgSbTe_2$ aligns with previous studies that identify it as exhibiting glass-like ultralow intrinsic thermal conductivity, attributed to the strong anharmonicity in the defects, stacking faults, and spontaneously formed nanoscale impurity phase.*[6,7,15,18,20] *In contrast, Sn-doped $AgSbTe_2$ demonstrates higher κ values compared to the pristine material. This increase is primarily due to enhanced electronic thermal conductivity (κ_e) and a slight elevation in κ_L. The increase in κ_L can be attributed to the elimination of the nanostructed Ag_2Te impurity phase upon Sn doping, which reduces phonon scattering centers and consequently allows for more efficient heat transport through the lattice. While previous studies on Hg,*[21] *Yb,*[22] *and Cd*[20] *doping in $AgSbTe_2$ have reported decreases in lattice thermal conductivity, our study observes an increase in κ_L suggesting that the specific nature of the*

doping element and its interactions within the matrix play a critical role in determining the overall thermal behavior." (*Line 13, Page 31*)

Response–to–Referees letter

Reviewer #1:

The authors have made commendable efforts to improve the work and have added substantial experiments to address my question. However, I still have one minor question: Regarding device simulation: It is unusual that the simulated power output exceeds the measured power, while the simulated efficiency aligns with the measured efficiency. Could the authors provide a more detailed comparison between simulated and experimental values, including open-circuit voltage, internal resistance, power, heat flow, and efficiency across different temperature differences? This would offer readers a clearer understanding of the device's performance.

We sincerely thank Reviewer #1 for the valuable feedback, which has helped enhance the clarity and depth of our manuscript. The suggested comparison is indeed critical for fully conveying our findings, and we appreciate the opportunity to clarify these aspects further.

In response, we have added a detailed comparative analysis between simulated and experimental data for key performance metrics, including open-circuit voltage (V_{oc}), internal resistance, power output (P_{max}), heat flow (Q_{in}), and efficiency (η) across a range of temperature differences. These new plots (Figure S16a) offer a comprehensive side-by-side view of the simulated and experimental results, providing a clearer understanding of the device's performance.

As noted by the reviewer, our simulations predict slightly higher values than the experimental measurements for power output (Figure S16c), open-circuit voltage (Figure S16a), internal resistance (Figure S16b), and heat flow (Figure S16e). We attribute these discrepancies to differences in the input parameters and boundary conditions applied in the COMSOL simulations, which may not fully capture real-world conditions such as interfacial losses, contact resistance, or other subtle factors. Despite these minor deviations, the simulated maximum efficiency aligns closely with the experimental value, with a simulated efficiency of 12.2% and an experimental efficiency of 12.1% (Figure S16f), underscoring the reliability of our model in capturing the overall device behavior.

Action: The manuscript and SI have been revised accordingly.

"The device performance was further validated by simulations of internal resistance, V_{oc}, P_{out}, Q_{in} and η, based on the dimensions of the p/n legs and their transport properties. The simulation results (Figure S16) demonstrated slightly higher, yet comparable values for V_{oc}, P_{max}, η_{max}, and power density when compared to experimental data. These minor discrepancies are associated with deviations in input parameters or boundary conditions applied in the simulation, supporting the reliability and consistency of the experimental measurements." (*Page 16, Line 4*)

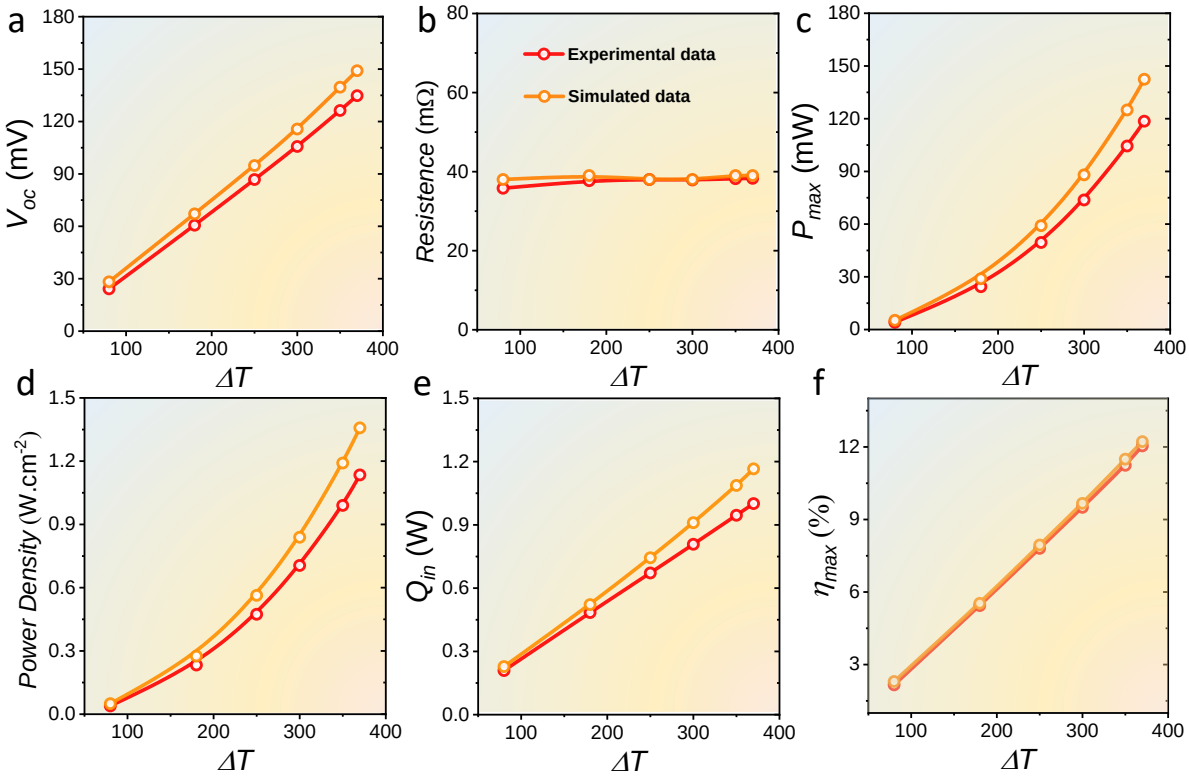

Figure S16-2. Comparison of experimental data (red color) with the data from COMSOL Multiphysics simulation software (orange color) on the unicouple device made of $AgSb_{0.94}Sn_{0.06}Te_2$ leg and $Yb_{0.25}Co_{3.75}Fe_{0.25}Sb_{12}$ leg: (a) open-circuit voltage, V_{oc}; (b) internal resistance; (c) power output, P_{max}; (d) power density; (e) heat flow, Q_{in} and (f) efficiency, η_{max}.

Additionally, please highlight the revisions made in the manuscript, as it is currently difficult for me to identify the updated sections.

To ensure that our revisions are easily identifiable, we have uploaded a version of the manuscript with all changes highlighted in yellow (file named *manuscript_changes highlighted in yellow*). This provides a convenient guide for the reviewer to track the updates and added discussions.

Once again, we thank Reviewer #1 for the constructive suggestions, which have significantly improved the presentation of our findings.